Bulk heterojunction solar cells: the role of alkyl side chain on nanoscale morphology of sulfur overrich regioregular polythiophenes/fullerene blends.

Elisabetta Salatelli[±], Martina Marinelli[±], Massimiliano Lanzi[±], Alberto Zanelli[§], Simone Dell'Elce[§], Andrea Liscio[¥], Massimo Gazzano[§], Francesca Di Maria[§]**

[±] Dpt. of Industrial Chemistry Toso Montanari, University of Bologna, Viale Risorgimento 4, I-40163 Bologna, Italy

[§] CNR-ISOF, Via P. Gobetti 101, I-40129 Bologna, Italy

[¥] CNR-IMM, Via Fosso del Cavaliere 100, I-00133 Roma, Italy

KEYWORDS Sulfur overrich regioregular polythiophenes, head to head substitution regiochemistry, side-chain engineering, nanoscale morphology, air-processed bulk heterojunction solar cells.

ABSTRACT: Regioregular HH-TT poly(3,3'-thioalkylbithiophene)s bearing branched or linear alkyl side-chain substituents (PT2SR) have been synthesized and characterized in order to investigate their behavior, when used as electron donor components in blend with a fullerene derivative (PCBM) as electron acceptor, in air-processed photovoltaic solar cells with bulk heterojunction architecture. The optoelectronic characteristics, energy gap, nanoscale morphology and crystallinity of the blends (PT2SR/PCBM) were examined by UV–vis spectroscopy, cyclic

voltammetry, Kelvin Probe Force Microscopy and X-ray diffraction. We demonstrate that thioalkyl substituents are able to influence the PCBM self-assembly and the morphology of the polymeric film, important parameters to maximize the efficiency of solar cell. In particular, the presence of chemical branching in the side chain of the sulfur overrich polythiophene backbone favors the formation of PCBM clusters, of size about 100±30 nm as confirmed by X-ray diffraction and KPFM measurements, and facilitates the intermixing between the donor and acceptor materials at the nanoscale level, thus determining a corresponding increase in device performance.

1. INTRODUCTION

Polymeric solar cells (PSCs) based on conjugated semiconductor polymers and fullerene derivatives are attracting much attention in both academic and industrial research. Their unique advantages such as light weight, flexibility and low-cost fabrication over large areas make them a valuable alternative to conventional inorganic thin-film solar cells.[1,2] In particular, polymeric or oligomeric thiophene derivatives are being deeply investigated as donors blended with fullerene acceptors in bulk heterojunction (BHJ) solar cells reaching high efficiency.[3-6] Being this architecture essentially based on a bi-continuous network of electron-donor and -acceptor moieties in which the two components are separated at nanoscale level,[7] a subtle balance between high interfacial area of donor and acceptor moieties, while maintaining large enough domain size for charge transport to the electrodes, is involved. In this context, structural features such as size, type and position of side-chain substituents, as well as regioregularity of the polythiophene backbone, play a relevant role on nanoscale morphology of the active blend layer. Indeed, the alkyl side chain usually linked to the electron donor polymeric moiety, in addition to favor solubility, processability and compatibility with the fullerene acceptor, also affects the electronic properties, the crystallinity

degree and the overall physical structure of the material in the aggregated state. Thus, its accurate selection in order to achieve the optimal balance for maximum photoconversion efficiency (PCE) is required.[8] As far as the regioregularity of polyalkylthiophene derivatives is concerned, while the obtainment of head-to-tail (HT) regioregular polymeric derivatives requires handling of delicate synthetic procedures,[9,10] the preparation of head-to-head tail-to-tail (HH-TT) derivatives can be conveniently carried out through the popular iron trichloride oxidation procedure, starting from symmetrically substituted bithiophene monomers. Despite this, polymers containing only HH-TT junctions have been less investigated, since this regiochemistry favors backbone distortion and reduced electron delocalization. However, the introduction of an heteroatom such as sulfur, interposed between the thiophene ring and the alkyl substituent, enables to compensate by mesomeric effect for the loss of conjugation narrowing the energy gap between the highest occupied molecular orbital (HOMO) and the lowest unoccupied molecular orbital (LUMO) of the polythiophene derivative.[11] To the light of the above considerations, we report here the synthesis and characterization of a novel class of *sulphur overrich* polymeric derivatives based on bithiophene repeating units, all exclusively featured by HH-TT junctions in the main chain, namely poly-3,3'-bis(thiohexyl)-2,2'-bithiophene (PT2Shex), poly-3,3'-bis[thio(1-methylpentyl)]-2,2'-bithiophene (PT2Sbr1) and poly-3,3'-bis[thio(2-ethylhexyl)]-2,2'-bithiophene (PT2Sbr2). Linear or differently branched thioalkyl side-chain substituents were introduced in the above derivatives in order to investigate their effect on solid state morphology, when blended with the fullerene derivative [6,6]-phenyl-C_{61}-butyric acid methyl ester (PCBM), and consequently on their photovoltaic properties when employed in BHJ solar cells. The structural, electrochemical and photophysical properties of the polymers were investigated by gel permeation chromatography (GPC), differential scanning calorimetry (DSC), thermogravimetric analysis (TGA), ^{1}H-NMR,

UV-Visible and photoluminescence (PL) spectroscopy, X-rays diffraction (XRD) and cyclic voltammetry (CV). Blends of the polymeric samples as electron-donor moieties with PCBM, as the electron-acceptor, were characterized by CV, XRD, Kelvin Probe Force Microscopy (KPFM) and finally deposited and tested under ambient air conditions in BHJ polymeric solar devices by current-voltage (J-V) measurements under illumination.

2. EXPERIMENTAL SECTION

2.1 Synthesis and characterization. All synthetic details are given in Supporting Information**.** All air- or moisture-sensitive reactions were performed under argon in dried glassware. All reagents and solvents were purchased from Aldrich Chemical Co. and used as received unless otherwise specified. ^{1}H-NMR spectra were recorded at room temperature in $CDCl_3$ solutions using a Varian Mercury 400 (400 MHz) spectrometer; chemical shifts are reported in ppm units with TMS as the internal standard. UV-Vis absorbance and PL spectra were recorded on a Perkin Elmer Lambda 20 and Perkin Elmer LS50B spectrophotometers, respectively, at room temperature on 1.3×10^{-3} M chloroform solutions using 1 cm quartz cells. Average molecular weights and polidispersity of the polymers were determined by GPC in THF solution on a HPLC Lab Flow 2000 apparatus equipped with a Rheodyne 7725i injector, a Phenomenex Phenogel mixed bed 5μ MXL type column and an UV-Vis detector Linear Instrument UVIS-200 operating at 254 nm. The calibration curve was recorded using monodisperse polystyrene standards. A DSC TA Instruments Q2000 operating in the –50÷250°C temperature range at a rate of 10°C/min under nitrogen atmosphere was used for the thermal analysis. A TGA TA Instruments Q600 was employed to assess the decomposition temperature of the polymers in the 20÷800°C temperature range at a heating rate of 20°C/min under nitrogen atmosphere.

2.2 Cyclic Voltammetry (CV). CV measurements were performed at 0.1 V/s on polymer thin films or the blends cast from a 0.1 M methylene chloride solution on ITO electrodes (2.25 cm^2) at room temperature, in propylene carbonate (Aldrich, anhydrous, stored under Ar pressure) 0.1 M $(C_2H_5)_4NBF_4$ (Aldrich, puriss. vacuum dried) as supporting electrolyte. The electrochemical cell was a home-made three-compartments cell equipped with a Pt wire auxiliary electrode and an aqueous KCl Saturated Calomel reference Electrode (SCE) connected to the working compartment with a liquid bridge (-0.500 V vs. Fc/Fc^+). The solution was purged with Ar before the measurements and maintained under Ar pressure. The CV curves were recorded using an AMEL model 5000 potentiostat/galvanostat controlled by the software Corrwere 2.9 for Windows. HOMO, LUMO and band gap (E_g) energies were estimated on the basis of the following relationships: $E_{HOMO} = -(E_{ox} + 4.68)$, $E_{LUMO} = -(E_{red} + 4.68)$, $E_g = -(E_{HOMO} - E_{LUMO})$. Calculated values are expressed in eV units.[12]

2.3 X-ray diffraction (XRD). XRD patterns were obtained with CuK_α radiation (λ = 1.5418Å) in reflection mode by means of an X'Pert PANalytical diffractometer equipped with a fast X' Celerator detector, 0.066° and 80s /step. The samples were analyzed as cast films obtained over glass slides. The length of the coherent domains was evaluated from XRD data by using the line broadening. The width at half maximum intensity (b1/2) of the reflection at $2\theta = 10.8°$ was applied in the Scherrer equation:[13] $L = \frac{K\lambda}{\beta \cdot cos\theta}$, where K is the shape factor depending on crystal habit (chosen as 0.9), λ is the photon wavelength as discussed below, θ and β correspond to the position (i.e. the Bragg angle) and the line broadening at half the maximum intensity (FWHM) of the diffraction peak. The peak *111* of a silicon standard was used to evaluate the instrumental broadening.

2.4 Bulk heterojunction (BHJ) solar cells. BHJ solar cells were prepared according to the following procedure: the ITO glass substrate (2.5 × 2.5 cm^2, surface resistance 20 Ω/sq) was etched on one side by using a 10% wt. aqueous solution of HCl and heated at 60°C for 15 min in order to obtain a final area of 1.5 x 1.0 cm^2 covered by indium tin oxide. The substrate was then rinsed in turn with distilled water, 2-propanol, and finally dried by a gentle nitrogen flow. The final resistance of the ITO glass was 12 Ω/sq. Poly(3,4-ethylenedioxythiophene):polystyrene sulfonic acid (PEDOT:PSS, 2.8% wt., dispersion in water) was diluted 1:1 v/v with 2-propanol and the solution homogenized under mild sonication, filtered on a glass frit and finally deposited over the previously treated ITO glass by the doctor blading technique using a Sheen Instrument model S265674. The PEDOT:PSS film was heated in a Büchi GKR-50 glass oven at 120°C for 2h under vacuum. A solution made by mixing 5 mg of polymer and 5 mg of $PC_{61}BM$ in 2 ml of chlorobenzene was deposited in ambient air conditions by doctor blading technique on the glass slide in order to cover the PEDOT-PSS layer. The buffer and the active layers were then annealed at 120°C for 30 min and, finally, the Al electrode was deposited over the active layer through a shadow mask using an Edwards 6306A coating system operating at 10^{-6} mmHg. The prepared solar cells, having a final active area of 1.0 × 1.0 cm^2, were stored in the dark under nitrogen just before the performance testing procedure. The current-voltage characteristics were measured in air at room temperature using a Keithley 2401 source meter under the illumination of an Abet Technologies LS150 Xenon Arc Lamp Source AM 1.5 Solar Simulator (100 mW/cm^2), calibrated with an ILT 1400-BL photometer. The structure of the final device was: ITO (80 nm)/PEDOT:PSS (120 nm)/polymer:$PC_{61}BM$ (1:1 w/w) (120 nm)/Al (50 nm). Layer thickness was measured using a Burleigh Vista 100 AFM in a non-contact tapping mode. The reported photoconversion

efficiency results were averaged from ten measurements made under the same operating conditions.

2.5 Atomic Force Microscopy (AFM) and Kelvin Probe Force Microscopy (KPFM). AFM and KPFM measurements were obtained in air by employing a commercial microscope Multimode 8 (Bruker). In order to obtain a sufficiently large and detectable mechanical deflection, we used (k = 2.8 N/m) Pt/Ir coated cantilever silicon tips (SCM, Bruker) with oscillating frequencies in the range between 60 - 90 KHz. AFM and KPFM images are acquired in the same measurement; a topographic line scan is first obtained by AFM operating in Tapping Mode and then that same line is rescanned in Lift Mode with the tip raised to a lift height of 20 nm using the Frequency Modulation (FM) mode. KPFM provides a voltage resolution of about 5 mV, while the lateral resolution amounts to a few tens of nanometers. Higher lateral resolution is achieved in AFM amounting to few nanometers. The issue of the lateral resolution[14,15] and the application of AFM/KPFM technique in material science for opto-electronics[16,17] is comprehensively discussed in literature. The mean square roughness (R_{rms}) has been estimated by averaging the values obtained on several 10×10 μm^2 images acquired on different regions of the sample (corresponding to about 500 μm^2 of sampled surface). Raw AFM and KFPM data were treated by using histogram flattening procedures[18] to remove the experimental artifacts due to the piezo-scanners.

3. RESULTS AND DISCUSSION

3.1 Synthesis and characterization of polymers. The synthesis of monomeric 3,3'-bis(thioalkyl)bithiophenes T2Shex, T2Sbr1 and T2Sbr2 was previously carried out by us, via microwave-assisted Suzuki-Miyaura reaction of the related 2-Br-3-thioalkyl thiophene (TSRBr) precursors in the presence of bis(pinacolato)diboron and Pd(dppf)Cl_2.[19,20] Starting from the same precursors, an alternative simple and low-cost method based on BuLi/$CuCl_2$ oxidative coupling

has been adopted here (Scheme 1).[21] Through this way T2SHex and T2Sbr2 were obtained in high yields (see Supplementary Information) while T2Sbr1 was synthesized using the aforementioned Suzuki-Miyaura procedure, since the yield obtained with the copper catalyzed route was unsatisfactory. The bithiophene monomers T2SR were then polymerized by a simple and straightforward procedure such as the oxidative coupling with $FeCl_3$ (Scheme 1).[22]

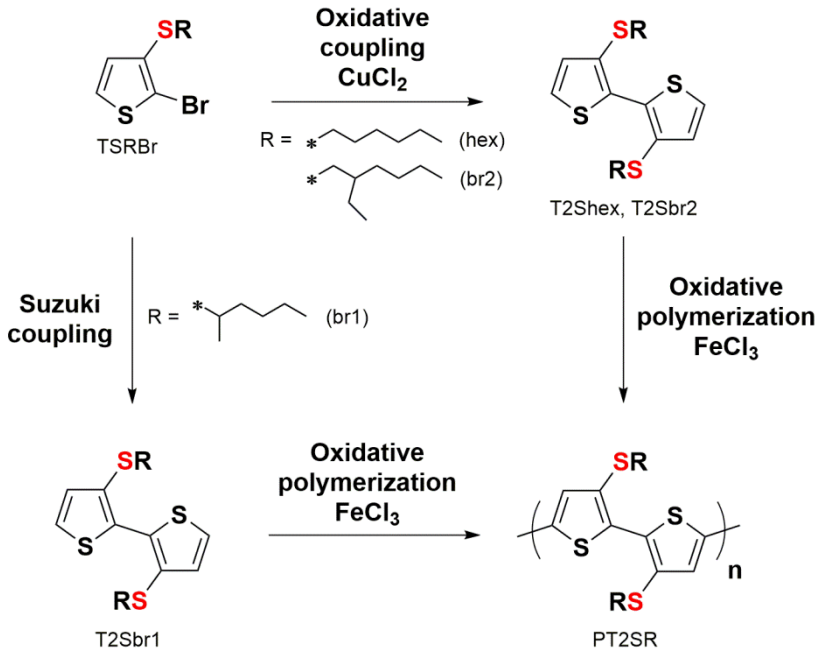

Scheme 1. Synthesis of *sulfur overrich* polythiophenes (PT2SR).

Although this procedure is a non-regiospecific method when applied to 3-alkylthiophenes, leading to polymers containing about 75% of HT linkages,[23] it allows to obtain completely regioregular polymers starting from symmetrically β-substituted bithiophenes, as a consequence of the chemical equivalence of the coupling positions. Therefore, the obtained polymeric derivatives exclusively display HH-TT junctions. In addition, the iron trichloride polymerization procedure has also advantages, such as simple handling and possibility to obtain the final product in the more conductive doped form. However, while PT2Sbr1 and PT2Sbr2 resulted almost

completely insoluble in CH_3OH, the poor solvent commonly employed for precipitation of the macromolecular crude material and purification from low molecular weight impurities, the crude PT2Shex displayed a significant solubility in CH_3OH. Indeed, the GPC analysis (Table 1) demonstrated that the polymerization of T2SHex actually occurred only to a limited extent, yielding an oligomeric derivative – from here on PT2Shex(1) – possessing an average polymerization degree of ca. 2.5, in terms of bithiophenic co-units. The ^{1}H-NMR spectrum (Figure 1S in Supplementary Information) also evidenced the presence of resonances related to the terminal rings protons in approximately the same amount as the isolated ring protons of the chain, indicative of an average chain length corresponding to only two bithiophenic repeating units. Consequently, in order to have a sample of PT2Shex with molecular mass and polydispersity similar to those of the branched polymers described herein, we used the previously adopted route,[24] i. e. the polymerization of 5,5'-dibromo-3,3'-bis(thiohexyl)-2,2'-bithiophene in the presence of bis(pinacolato)diboron and $PdCl_2$dppf (PTShex(2), Table 1). The DSC thermograms of the polymers (Table 1) display in the second heating cycle only a second–order phase transition ascribable to glass transition in the 50–71°C range, which appears related to the polymerization degree. The absence of melting transitions at higher temperatures clearly suggests the essentially amorphous character of these materials. All the samples show a similar behavior when submitted to thermal treatment carried out by TGA, with an initial weight loss starting around 170°C, originated by the side chains degradation. A second weight loss taking place above 300°C is attributed to starting decomposition of the polymeric backbone also.

Table 1. Yields and characterization data of polymeric derivatives.

	Yield (%)[a]	M_n *(g/mol)*[b]	M_w/M_n[c]	x_n[d]	T_g *(°C)*[e]	T_d *(°C)*[f]

PT2Shex(1)	97	1000	2.1	2.5	50	168
PT2Shex(2)	30	8040	2.0	20.1	61	260
PT2Sbr1	96	8300	1.9	20.9	71	282
PT2Sbr2	98	8700	1.9	19.2	67	187

[a] Weight polymer/weight monomer x 100. [b] Average molecular weight determined by GPC in THF. [c] Polydispersity index. [d] Average polymerization degree in terms of bithiophenic repeating units. [e] Glass transition temperature determined by DSC. [f] Decomposition temperature determined by TGA after 2% weight loss.

3.2 Optical properties. The absorption and emission spectra of bithiophene monomers and polymers were measured in $CHCl_3$ solution (Figure 1A and 1B). Similar featureless absorption and emission spectra are observed for all the monomers with comparable maximum absorption and emission wavelengths related to the $\pi-\pi^*$ electronic transition of the conjugated aromatic system. The poor dependence of the optical profile from the kind of side chain suggests that the monomers preferentially assume a similar anti coplanar conformation, assisted by weak sulfur-sulfur non bonding interactions.[24] Passing from monomers to polymers, a remarkable red-shift of λ_{max}, of the order of 180-190 nm for PT2Sbr1 and PT2Sbr2, indicative of increased electron delocalization along the backbone, is observed.

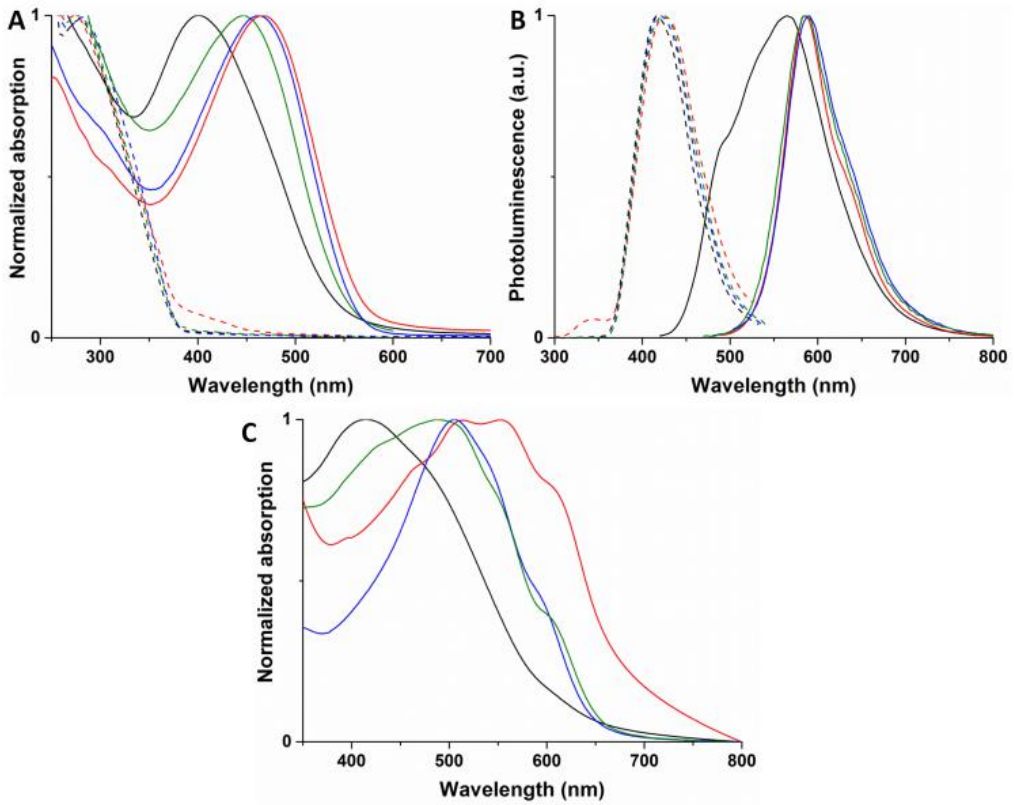

Figure 1. Normalized absorption (A) and photoluminescence (B) spectra in $CHCl_3$ of T2SR (black dashed line: T2Shex; red dashed line: T2Sbr1; blue dashed line: T2Sbr2) and PT2SR (black full line: PT2Shex(1); green full line: PT2Shex(2); red full line: PT2Sbr1; blue full line: PT2Sbr2). (C) Normalized absorption spectra of PT2SR as cast films from $CHCl_3$ (black full line: PT2Shex(1); green full line: PT2Shex(2); red full line: PT2Sbr1; blue full line: PT2Sbr2).

It is also to be noted that the lower red-shift (ca. 130 nm) of PT2Shex(1), compared to the other samples, confirms its low polymerization degree, as assessed by GPC and ^{1}H-NMR. However, the absorption maximum wavelength of PT2Shex(2) was still lower in comparison to the values exhibited by PT2Sbr1 and PT2Sbr2, thus suggesting that more extended electronic conjugation is achieved by the side-chain branched derivatives. It is also worth stressing the remarkable bathochromic shift of the maximum absorption due to the mesomeric effect provided by sulfur in these thiohexyl polymeric derivatives with respect to the related HH-TT polymer bearing the hexyl substituent directly linked to thiophene ring, characterized by a λ_{max} value of 378 nm only.[24] All

compounds are characterized by large Stokes shifts from absorption to emission (Table 2). In particular, the Stokes shifts of the polymers decrease in the order PT2Shex(1) > PT2Shex(2) > PT2Sbr2 > PT2Sbr1 suggesting a more planar and rigid conformation in solution for the last sample.

Table 2. Maximum absorption (λ_{max}) and emission (λ_{PL}) wavelengths (nm) of monomers and polymers in $CHCl_3$ solution.

Monomers	λ_{max}	λ_{PL}	*shift*	*Polymers*	λ_{max}	λ_{PL}	*shift*
T2Shex	267	415	148	***PT2Shex(1)***	400	567	167
T2Sbr1	273	423	150	***PT2Shex(2)***	448	586	138
T2Sbr2	279	418	139	***PT2Sbr1***	466	584	118
				PT2Sbr2	461	590	129

As shown in Figure 1C, an additional bathochromic shift of λ_{max} with respect to the absorptions in solution is displayed by the thin films of the polymers, attributable to an increase of the mean electronic conjugation length originated by the assumption of more ordered and planar conformations of the backbone in the solid state. This is also confirmed by the appearance of a vibronic structure related to the presence of strong inter- and intra-molecular interactions. In particular, PT2Sbr1 (λ_{max} 512 and 552 nm) displays the highest red-shifted and most structured absorption band with respect to PT2Shex(1) (λ_{max} 415 nm), PT2Shex(2) (λ_{max} 492 nm) and PT2Sbr2 (λ_{max} 505 nm). The presence of a significant degree of coplanarity in the solid state can be ascribed to reduced steric hindrance by the thioalkyl chains at the head-to-head junction of bithienyl units, in good agreement with the observation that thioalkyl substituents linked to HH-TT bithienyl co-units allow for backbone planarization in oligo- and polyalkylthiophenes.[25,26]

3.3 Electronic properties. The behavior of the polymers was investigated by cyclic voltammetry (CV) on solid films cast on ITO electrodes. As represented in Figure 2A, the oxidation waves of the polymers have similar onset potentials even if the shape of the waves appear quite different, probably due to different morphologies of the films and contact with the electrode.[19,27]

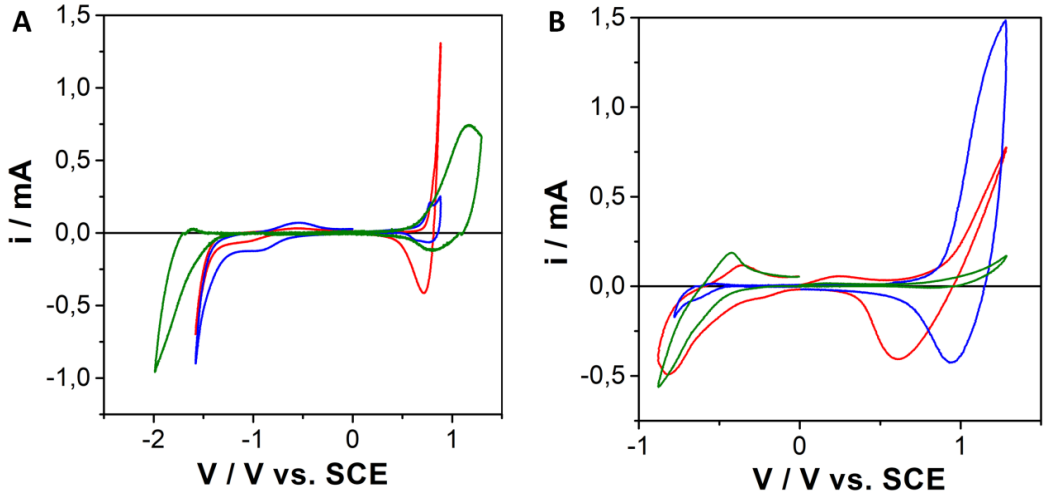

Figure 2. Second cyclic voltammograms in the solid state at 0.1 V s^{-1} of PT2Shex(2) (green line), PT2Sbr1 (red line) and PT2Sbr2 (blue line) (A) and their corresponding blends (B).

However PT2Shex(2) exhibits fair reversibility in the anodic region and an oxidation maximum at 1.15 V, higher than that already reported for electrochemically synthesized poly(3,3'-dialkylsulfanyl-2,2'-bithiophenes),[28] it also shows the most negative potential onset of the reduction wave, as reported in Table 3. PT2Sbr1 and PT2Sbr2 show similar onset oxidation potentials but different onset potentials of the reduction waves, displaying slightly higher values of E_{ox}^{onset} and less negative (of 0.13 and 0.09 V, respectively) values of E_{red}^{onset}, with respect to PT2Shex(2) (Table 3).

Table 3. Redox potentials[a], HOMO/LUMO energy levels[b] and electrochemical energy gap values[b] of the polymers and the corresponding blend with PCBM (1:1 w/w).

Sample	E_{ox}^{onset}	E_{red}^{onset}	*HOMO*	*LUMO*	E_g
PT2Shex(2)	0.70	–1.52	–5.38	–3.16	2.22
PT2Sbr1	0.73	–1.39	–5.41	–3.29	2.12
PT2Sbr2	0.72	–1.43	–5.40	–3.25	2.15
PT2Shex(2)/PCBM[d]	1.00	–0.49	–5.68	–4.19	1.49
PT2Sbr1/PCBM[d]	0.85	–0.48	–5.56	–4.20	1.33
PT2Sbr2/PCBM[d]	0.91	–0.48	–5.59	–4.20	1.39
PCBM				–4.00[c]	

[a] In V vs. SCE.[b] In eV. [c] Data from ref. 27. [d]After thermal annealing.

In particular, PT2Sbr1 results to be significantly easier to reduce than PT2Sbr2 indicating that its structure favors the overlapping of LUMO,[19,27] thus decreasing its energy down to –3.29 eV. As a result a lowering of the energy gap of PT2Sbr1 compared with PT2Shex(2) and PT2Sbr2 is observed. The electrochemically assessed E_g values are in good agreement with the absorption spectra of the films reported in Figure 1, with PT2Sbr1 showing the most red-shifted λ_{max} value. Thus, the energy of the frontier orbitals of PT2Sbr1 appears to well match with the energy level of PCBM for the coupling in an organic bulk heterojunction photovoltaic cell.

We also determined the energy levels and hence the effective energy gap in polymer:PCBM blends (Figure 2B), since the shift in the polymer HOMO and fullerene LUMO strictly depends on the blend composition and provides an important driving force for separating charge carriers.[29] We observed that the effect of the blend (PT2SR/PCBM 1:1 w/w) induces a variation, of the order of hundreds mV, in the onset of polymers oxidation wave compared to their levels in pure films (Table 3).

However, while the shift of the fullerene LUMO remains roughly the same in the three blends, the HOMO of the polymers increases of about 1 eV in the order PT2Shex(2) > PT2Sbr2 > PT2Sbr1, suggesting a more extended conjugation length for PT2Sbr1. This entails that the blend formed by PT2Sbr1/PCBM shows the shortest gap between the donor and the acceptor energy levels in comparison with the other two blends (PT2Sbr1/PCBM < PT2Sbr2/PCBM < PT2Shex(2)/PCBM). Moreover, it exhibits balanced currents of the reduction and oxidation waves indicating a better connection of blend components to ITO substrate.

3.4 Diffraction properties. The X-ray diffraction profiles of films cast from $CHCl_3$ of PT2Shex(2), PT2Sbr1 and PT2Sbr2 are reported in Figure 3B. All samples give rise to analogous X-ray diffraction patterns with a peak in the low angle region and a broad halo in the 15–35° interval. Differently from the related polymeric alkyl derivatives lacking the sulfur atom in the side chains, which display a tendency to produce amorphous domains in the solid state,[30] the above thioalkyl derivatives are characterized by the presence of some crystalline domains probably favored by a more planar conformation in the solid state driven by intra- and intermolecular sulfur-sulfur non bonding interactions.[19] The peak at $2\theta = 5.05°$ (d = 1.74 nm) for the PT2Shex(2), is ascribable to the distance of the almost parallel polythiophene chains belonging to the same plane and shifts to higher angles (shorter distances) for the branched ones: 5.23° (d = 1.69 nm) for PT2Sbr2 and 6.17° (d = 1.43 nm) for PT2Sbr1 (Figure 3A). The sharpest peak for PT2Sbr2 gives evidence of a better regularity in chain distance, whereas PT2Sbr1 appears to be the one with the worst overall order. The broad halo, that results from non regular distances between the alkyl chains and between the planes where thiophene chains lie, is almost invariant in all samples. The XRD profiles of the 1:1 (w/w) blends with PCBM are reported in Figure 3C. In all three samples, the low angle reflections belonging to the polymers disappear, suggesting that PCBM inhibits the

regular spacing of polythiophene chains and intercalates between them forming intermixed domains of amorphous polymer and PCBM. However, in the blend PT2Sbr1/PCBM several peaks, ascribable to the presence of a separate phase of PCBM, are present. This last sample appears therefore to be the only one exhibiting partially crystalline domains of PCBM clusters, estimated to be 85±15 nm, dispersed within the amorphous bulk of the material.

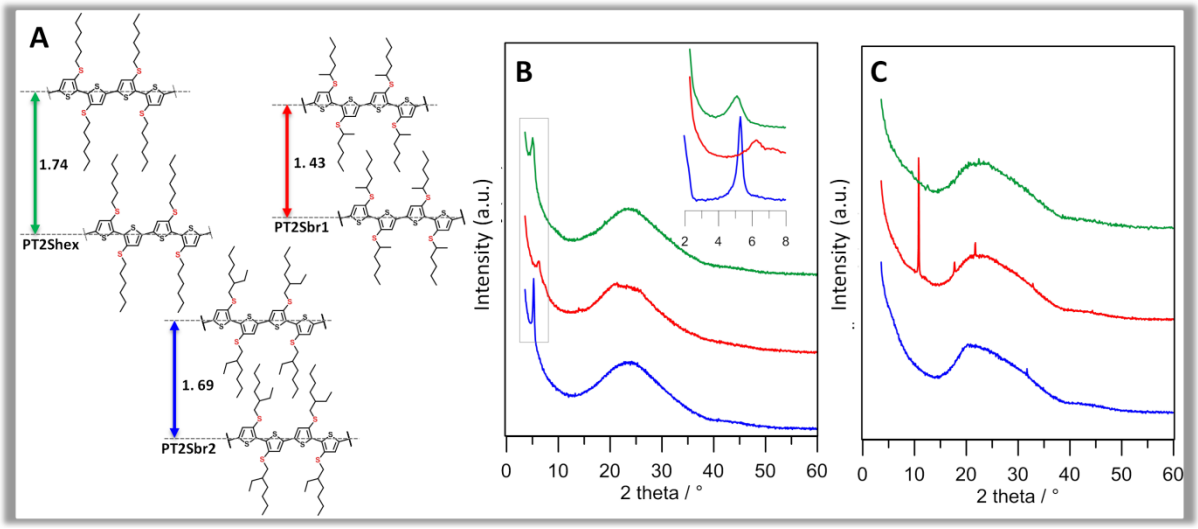

Figure 3. A) Proposed model for the supramolecular organization of polymers; the values of the interplanar distances are in nm. B) X-ray diffraction patterns of films of PT2Shex(2) (green line), PT2Sbr1 (red line), PT2Sbr2 (blue line) (inset: scan performed with narrower slits of the angular region) and C) their corresponding blends with PCBM (1:1 w/w), after thermal annealing.

3.5 Morphology and charge separation of PT2SR/PCBM blends. In order to investigate the effect of the chemical functionalization of the polymers on the blend morphology at the nanoscale level and how differences in morphologies may determine possible surface potential changes, AFM and KPFM measurements were carried out. Characterization of the morphology of the blends at the microscale level performed by AFM shows that PT2Shex(2):PCBM and PT2Sbr2:PCBM blends (Figure 4a,e) are more uniform (mean square roughness (R_{rms}) values amount 5±1 nm and 3±1 nm, respectively) than that formed by PT2Sbr1:PCBM (Figure 4c) (R_{rms} = 50±20 nm), which

exhibits micrometric size clusters. R_{rms} values and relative standard deviations are calculated mapping AFM images on 10×10 μm^2 scale (1024×1024 pixel).

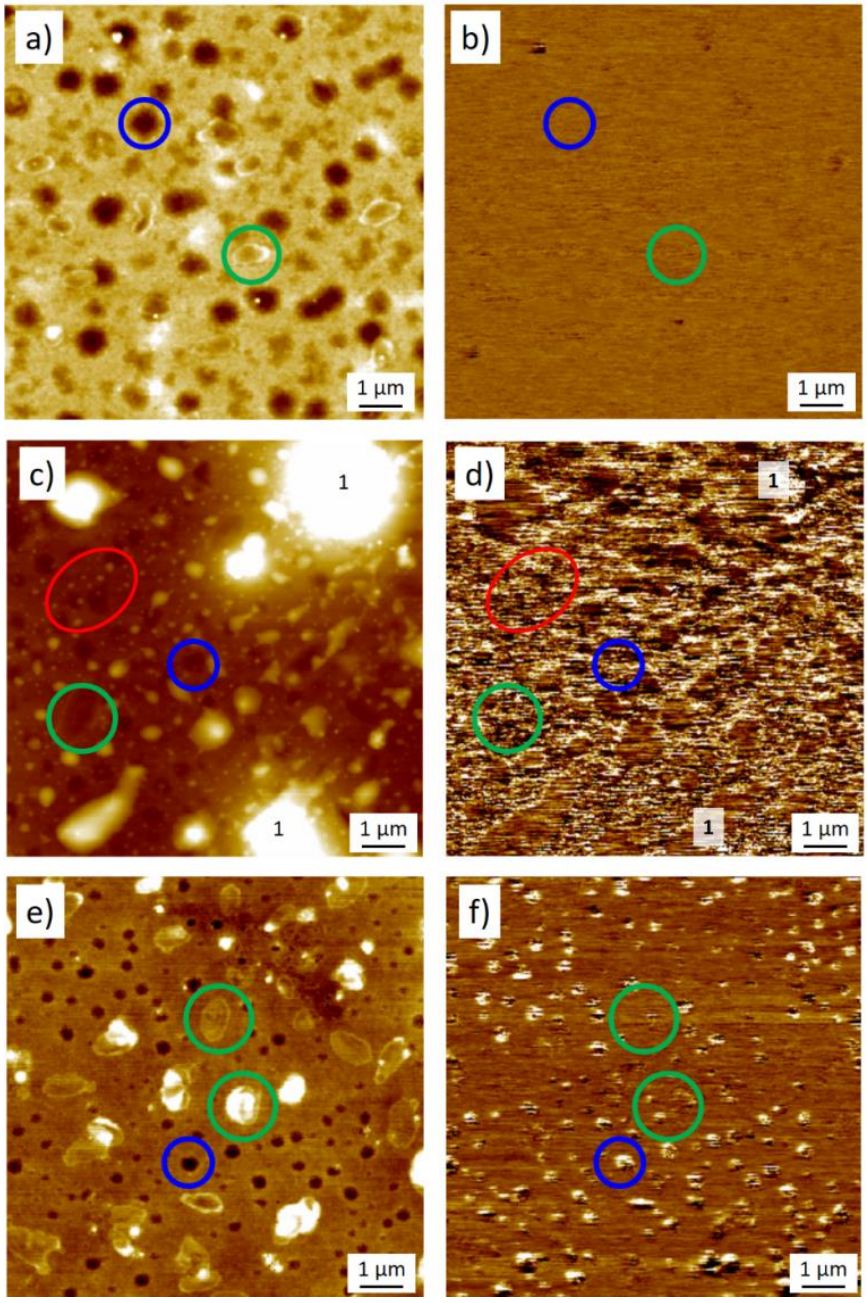

Figure 4. AFM morphology and corresponding KPFM images of PT2Shex(2):PCBM (a, b), PT2Sbr1:PCBM (c, d) and PT2Sbr2:PCBM (e, f). Z-ranges: 15 nm (a, e), 150 nm (c) and 200 mV (b, d, f).

The surfaces of PT2Shex(2):PCBM (Figure 4a) and PT2Sbr2:PCBM (Figure 4e) are quite uniform, exhibiting holes (marked by blue circles) with different diameters of 500±80 nm and 180±80 nm, respectively, and 10±1 nm deep. Moreover, in both samples additional flat aggregates of ca. 1 μm size (marked by green circles), that can be addressed to a further rearrangement due to solvent evaporation, are present. Conversely, the surface of the PT2Sbr1:PCBM blend (Figure 4c) is more complex, since additional large structures with broadened profiles (labeled with 1) and aggregates of 100±30 nm diameter (marked by red ellipse) corresponding to PCBM clusters, are also present, in agreement with XRD results.

KPFM images map the surface photo-voltage (SPV) measured as difference between the surface potential under illumination and in the dark: $SPV = SP_{light} - SP_{dark}$. Mapping the photo-induced charge density at the nanometric scale, KPFM images show the photo activity of the blend directly visualizing the formation of the photo-induced charges at the electron donor-acceptor interface.[31] the measured potentials are reported using the same false color scale and color range. As shown in Figure 4b, d and f, a clear difference in surface potential in the three samples is observed. Only the blends formed by the polymers bearing branched side chain, PT2Sbr1 and PT2Sbr2 (Figure 4d and 4f), show photo-voltage activity. In particular we observed that PT2Sbr2 shows potential variation only inside the hole while the top film does not change potential between light and dark, whereas PT2Sbr1 shows spread differences of ca 200 mV over the whole surface. This evidence suggests the presence of a good intermixing between PCBM and the polymeric film at the scale 10-20 nm, lower than the lateral resolution of the KPFM technique; as confirmed by qualitative comparison of the corresponding phase maps of the three systems (see figure 2S). Only PT2Sbr2 phase image presents a complex phase contrast revealing the presence of *in-plane* phase separation. Differently, the phase maps of the other two blends are more uniform, as expected in the case of *out-of-plane*

phase separation (i.e. layered structure).**3.6 Bulk heterojunction solar cells.** The PT2SR derivatives blended with PCBM (1:1 w/w) were tested as active media in solution-processed in air BHJ devices. Thermal annealing was performed on the devices, since it has been reported that it can improve the performances of devices fabricated in air.[32] To investigate this effect, the absorption spectra of thin films of the blends before and after annealing, at 120°C for 30 min., were recorded (Figure 5).

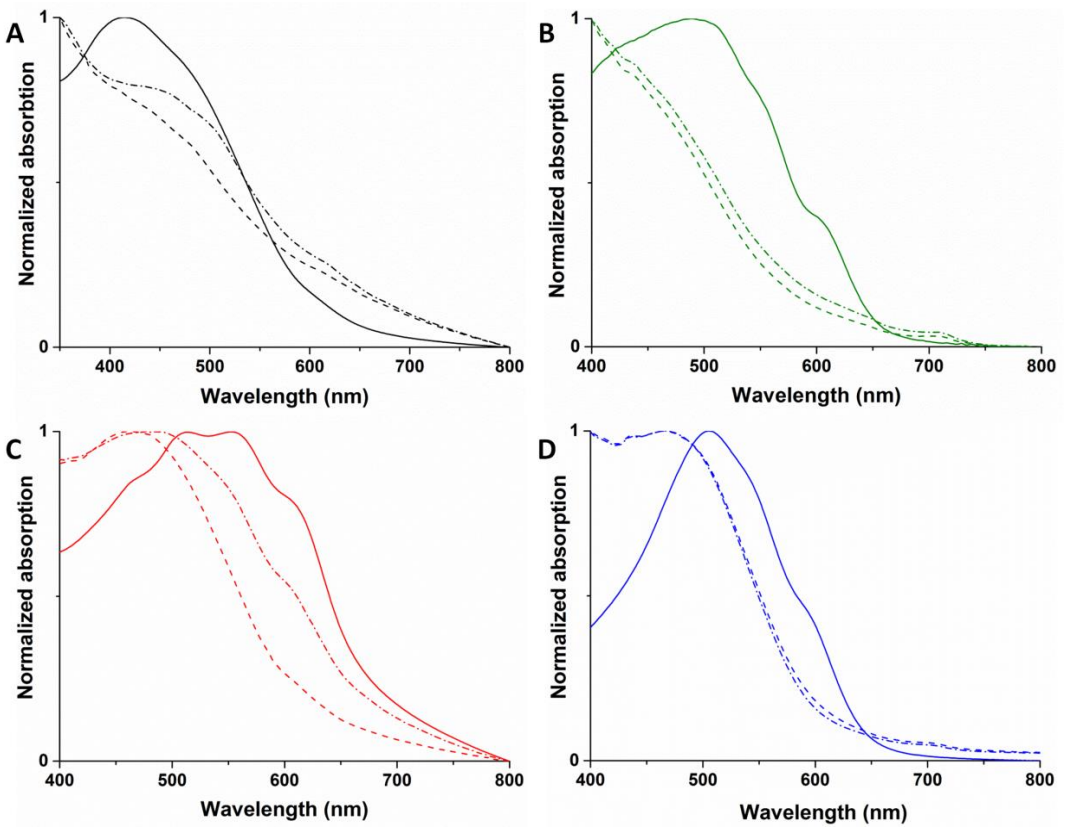

Figure 5. Normalized absorption spectra of PT2SR/PCBM blends (1:1 w/w) before (dashed line) and after (dashed-dot line) annealing of PT2Shex(1) (A), PT2Shex(2) (B), PT2Sbr1 (C) and PT2Sbr2 (D). For comparison the spectra of pure polymer films are reported as full lines.

It appears that the presence of PCBM in the blend originates the reduction or even the disappearance of the vibronic bands shown by the pure polymeric sample, suggesting initial

disruption of ordered structures in the bulk. However, more structured bands are produced upon annealing for PT2Shex(1) and PT2Sbr1 (Figure 5a and 5c, respectively), indicating a better tendency to give inter- and intra-molecular interactions in the bulk. Minor spectral effects are instead produced by annealing the blends of PT2Shex(2) and PT2Sbr2 (Figure 5b and 5d, respectively).

The J-V features of solar cells with structure ITO/PEDOT:PSS/PT2SR:$PC_{61}BM$/Al are reported in Figure 6 and the photovoltaic parameters listed in Table 4.

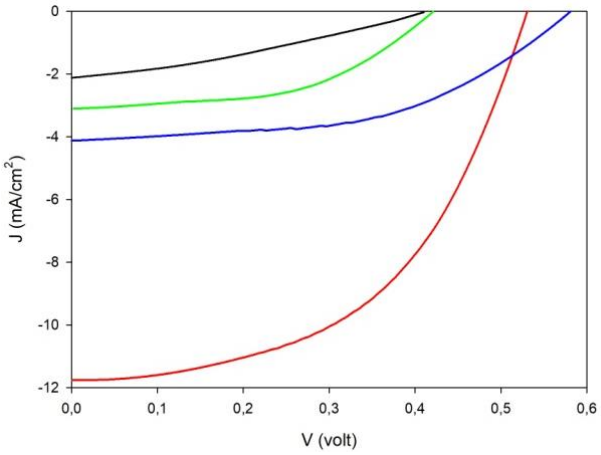

Figure 6 J-V curves under illumination of the solar cells prepared with PT2Shex(1) (black line), PT2Shex(2) (green line), PT2Sbr1 (red line) and PT2Sbr2 (blue line).

As evidenced, the device containing the photoactive component PT2SHex(1) shows the lowest efficiency, which improves upon increasing the average chain length, as shown by PT2SHex(2), likely in consequence of enhanced conjugation extent in the backbone. It is to be noted that the presence of the sulfur atom in the side chain of PT2Shex(1) and (2) anyway allows to recovery PCE values with respect to the related HH-TT polymeric derivative lacking of the extra sulfur atom, which was proved to be actually photoinactive.[24] The presence in the sulfur overrich polythiophene of branched side chains appears however to favor the cell efficiency to some extent.

In particular, the best performance is obtained for PT2Sbr1, which showed the lowest E_g value, a more structured optical absorptions and, as confirmed by XRD and KFPM measurements, a partially ordered arrangement of the electron acceptor PCBM. The relevance of the occurrence of ordered aggregation of PCBM favoring the increase of PCE has indeed been previously highlighted, since it may significantly decrease the recombination rate and at the same time increase the charge carrier mobility by favoring the correct percolation pathway of holes to ITO electrode and electrons to Al electrode, as indicated by the CV shape.[33,34] The more efficient behavior of both the branched polymeric samples with respect to the related PT2Shex samples**,** appears reasonably attributable to subtle variations of the physical arrangement assumed by the branched macromolecules in the solid state favoring the current photogeneration (related to J_{sc}) and/or the energy difference between donor and acceptor orbitals (related to V_{oc}). Sizeable variations of all parameters of photovoltaic devices related to structural changes of the alkyl substituent linked to the thiophene ring in thiophene copolymers have been attributed to morphology changes of the blends with the fullerene electron acceptor[35,36] and appear to be present in our sulfur overrich materials, also. In particular the highest values of J_{sc} observed for the blend PT2Sbr1/PCBM is probably to be ascribed to the simultaneous presence of nano- and microdomains, as evidenced by KPFM measurements.

In particular, it is noteworthy to underline that the highest performance is achieved in the case of rough active layer surface with large aggregates, which usually are a signs of aging and performance degradation. The achieved experimental evidence clearly indicates that: i) the aging effect can be neglected and ii) the performance increases with roughness corresponding to a larger specific surface area to inject and extract the photo-charges into electrodes.

Table 4. Properties of the BHJ solar cells prepared with polymeric derivatives

Sample	J_{sc} [a]	V_{oc} [b]	*FF* [c]	*PCE* [d]
PT2Shex(1)	2.1	0.41	46	0.40
PT2Shex(2)	3.1	0.42	48	0.62
PT2Sbr1	11.8	0.53	56	3.50
PT2Sbr2	4.1	0.58	55	1.30

[a] Short circuit current in mA/cm^2. [b] Open circuit voltage in V. [c] Fill factor in %. [d] Photovoltaic cell efficiency in %.

We finally observe that such materials are comparatively stable when exposed in air to optical radiation (an AM1.5 solar simulator), similarly indicating a high level of photostability. This promising result suggests that there may be significant scope to simplify an OPV manufacture process using air-based printing and processing techniques.

CONCLUSIONS

Novel fully regioregular HH-TT *sulfur overrich* polythiophenes bearing in the side chain branched alkyl moieties were synthesized in high yield, starting from the corresponding 3,3'-thioalkylbithiophene monomers, through oxidative polymerization with $FeCl_3$ avoiding the adoption of more complex synthetic procedures. The structural, electrochemical and photophysical properties of the above materials in blend with PCBM (1:1 w/w) have been investigated and compared to those of the related polymer with a linear thioalkyl substituent. Structural changes in the side chains of the polythiophene backbone allow the fine tuning of the absorption, energy levels, crystallinity and charge separation under illumination resulting in markedly different photovoltaic performances. In particular, KPFM characterization of the blends evidenced the favorable role played by the presence of side chain branching in the formation of both intimately intermixed domains of amorphous polymer and fullerene and pure clusters of PCBM. We ascribe this result to the combination of steric hindrance originated by branching and the presence of sulfur/sulfur non-bonding interactions that may drive the intra- and inter-chain interactions and

self-aggregation modalities of the material, favoring an interpenetrating network at the nanoscale level. Finally, the air-stability of these conjugated polymers is attractive, since manufacturing OPV devices in air may reduce the capital investment required to develop the necessary production infrastructure.

ASSOCIATED CONTENT

The Supporting_Information is available free of charge.

AUTHOR INFORMATION

Corresponding Author

*E-mail elisabetta.salatelli@unibo.it

*E-mail francesca.dimaria@isof.cnr.it

ACKNOWLEDGEMENTS

We are grateful to Prof. Luigi Angiolini for helpful discussion. The research leading to these results has received funding from the European Union's Horizon 2020 research and innovation programme (grant agreement n°696656 Graphene Flagship) and the EC Marie-Curie ITN- iSwitch (GA no. 642196).

REFERENCES

(1) Roncali, J.; Leriche P.; Blanchard, P. Molecular Materials for Organic Photovoltaics: Small is Beautiful. *Adv. Mater.*, **2014**, *26*, 3821─3838.

(2) Krebs, F. C.; Espinosa, N.; Hösel, M.; Sondergaard, R. R.; Jorgensen, M. 25th Anniversary Article: Rise to Power – OPV-Based Solar Parks. *Adv. Mater.*, **2014**, *26*, 29─39.

(3) Kan, B.; Li, M.; Zhang, Q.; Liu, F.; Wan, X.; Wang, Y.; Ni, W.; Long, G.; Yang, X.; Feng, H.; Zuo, Y.; Zhang, M.; Huang, F.; Cao, Y.; Russell, T. P.; Chen, Y. A Series of Simple Oligomer-like Small Molecules Based on Oligothiophenes for Solution-Processed Solar Cells with High Efficiency. *J. Am. Chem. Soc.*, **2015**, *137*, 3886─3893.

(4) Fitzner, R.; Mena-Osteritz, E.; Mishra, A.; Schulz, G.; Reinold, E.; Weil, M.; Körner, C. Ziehlke, H.; Elschner, C.; Leo, K.; Riede, M.; Pfeiffer, M.; Uhrich, C.; Baüerle, P. Correlation of π-Conjugated Oligomer Structure with Film Morphology and Organic Solar Cell Performance. *J. Am. Chem. Soc.*, **2012**, *134*, 11064─11067.

(5) Brabec, C. J.; Gowrisanker, S.; Halls, J. J. M.; Laird, D.; Jia, S.; Williams, S. P. Polymer–Fullerene Bulk-Heterojunction Solar Cells. *Adv. Mater.*, **2010**, *22*, 3839─3856.

(6) Heeger, A. J. Semiconducting polymers: the Third Generation. *Chem. Soc. Rev.*, **2010**, *39*, 2354─2371.

(7) Dou, L.; You, J.; Hong, Z.; Xu, Z.; Li, G.; Street, R. A.; Yang, Y. 25th Anniversary Article: A Decade of Organic/Polymeric Photovoltaic Research. *Adv. Mater.*, **2013**, *25*, 6642─6671.

(8) Guo, H.; Shen, T.; Wu, F.; Hou, R. R.; Liu, X.; Zhao, B.; Tan, S. Tuning the photovoltaic performances of the terpolymers based on thiophene-benzene-thiophene via the modification of alkyl side chains. *J. Appl. Polym. Sci.*, **2016**, 1, 42982.

(9) McCullough, R. D.; Lowe, R. D.; Jayarman, M.; Anderson, D. L. Design, synthesis, and control of conducting polymer architectures: structurally homogeneous poly(3-alkylthiophenes). *J. Org. Chem.*, **1993**, *58*, 904─912.

(10) Chen, T. A.; Wu, X.; Rieke, R. D. Regiocontrolled Synthesis of Poly(3-alkylthiophenes) Mediated by Rieke Zinc: Their Characterization and Solid-State Properties. *J. Am. Chem. Soc.*, **1995**, *117*, 233─244.

(11) Bundgaard, E.; Krebs, F. C. Low band gap polymers for organic photovoltaics. *Energy Mater. Sol. Cells*, **2007**, *91*, 954─985.

(12) Trasatti, S. The absolute electrode potential: an explanatory note. *Pure Appl. Chem.*, **1986**, 58, 955─966.

(13) Klug, H. P.; Alexander, L. E. New York: Wiley Interscience, **1974**.

(14) Liscio, A.; Palermo V.; Samorì, P. Probing Local Surface Potential of Quasi-One-Dimensional Systems: A KPFM Study of P3HT Nanofibers. *Adv. Funct. Mater.*, **2008**, *18*, 907─914.

(15) Liscio, A.; Palermo, V.; Samorì, P. Nanoscale Quantitative Measurement of the Potential of Charged Nanostructures by Electrostatic and Kelvin Probe Force Microscopy: Unraveling Electronic Processes in Complex Materials. *Acc. Chem. Res*., **2010**, *43*, 541─550.

(16) Melitz, W.; Shen, J.; Kummel, A. C.; lee, S. Kelvin probe force microscopy and its application. *Surf. Sci. Rep*., **2011**, *66*, 1─27.

(17) Musumeci, C.; Liscio, A.; Palermo V.; Samorì, P. Electronic characterization of supramolecular materials at the nanoscale by Conductive Atomic Force and Kelvin Probe Force microscopies. *Mater. Today*, **2014**, *17*, 504─527.

(18) Liscio, A. Scanning Probe Microscopy beyond Imaging: A General Tool for Quantitative Analysis. *ChemPhysChem*, **2013**, *14*, 1283─1292.

(19) Di Maria, F.; Olivelli, P.; Gazzano, M.; Zanelli, A.; Biasucci, M.; Gigli, G.; Gentili, D.; D'Angelo, P.; Cavallini, M.; Barbarella, G. A Successful Chemical Strategy To Induce Oligothiophene Self-Assembly into Fibers with Tunable Shape and Function. *J. Am. Chem. Soc.*, **2011**, *133*, 8654─8661.

(20) Di Maria, F.; Biasucci, M.; Di Nicola, F. P.; Fabiano, E.; Zanelli, A.; Gazzano, M.; Salatelli, E.; Lanzi, M.; Della Sala, F.; Gigli, G.; Barbarella, G. Nanoscale Characterization and Unexpected Photovoltaic Behavior of Low Band Gap Sulfur-Overrich-Thiophene/Benzothiadiazole Decamers and Polymers. *J. Phys. Chem. C.*, **2015**, *119*, 27200─27221.

(21) Mullen, K.; Wegner, G. Electronic Materials: The Oligomer Approach, *Wiley-VCH*, **1998**.

(22) Della Casa, C.; Bertinelli, F.; Costa Bizzarri, P.; Salatelli, E. Properties of a hydroxydecyl-functionalized polythiophene synthesized by the iron trichloride route. *Adv. Mater.*, **1995**, *7*, 1005─1009.

(23) Costa Bizzarri, P.; Andreani, F.; Della Casa, C.; Lanzi, M.; Salatelli, E. Ester-functionalized poly(3-alkylthienylene)s: substituent effects on the polymerization with $FeCl_3$. *Synth. Met.*, **1995**, *75*, 141─147.

(24) Di Maria, F.; Gazzano, M.; Zanelli, A.; Gigli, G.; Loiudice, A.; Rizzo, A.; Biasiucci, M.; Salatelli, E.; D'Angelo, P.; Barbarella, G. Synthesis and Photovoltaic Properties of Regioregular Head-to-Head Substituted Thiophene Hexadecamers. *Macromolecules*, **2012**, *45*, 8284─8291.

(25) Iarossi, D.; Mucci, A.; Schenetti, L.; Seeber, R.; Goldoni, F.; Affronte, M.; Nava, F. Polymerization and Characterization of 4,4'-Bis(alkylsulfanyl)-2,2'-bithiophenes. *Macromolecules*, **1999**, *32*, 1390─1397.

(26) Gentili, D.; Di Maria, F.; Liscio, F.; Ferlauto, L.; Leonardi, F.; Maini, L.; Gazzano, M.; Milita, S.; Barbarella, G.; Cavallini, M. Targeting ordered oligothiophene fibers with enhanced functional properties by interplay of self-assembly and wet lithography. *J. Mater. Chem.* **2012**, *22*, 20852─20856.

(27) Di Maria, F.; Fabiano, E.; Gentili, D.; Biasiucci, M.; Salzillo, T.; Bergamini, G.; Gazzano, M.; Zanelli, A.; Brillante, A.; Cavallini, M.; Della Sala, F.; Gigli, G.; Barbarella, G. Polymorphism in Crystalline Microfibers of Achiral Octithiophene: The Effect on Charge Transport, Supramolecular Chirality and Optical Properties. *Adv. Funct. Mater.*, **2014**, *24*, 4943─4951.

(28) Ng, S. C.; Miao, P. Electrochemical Synthesis and Characterization Studies of Poly[3,3'-dialkylsulfanyl-2,2'-bithiophene] Films. *Macromolecules*, **1999**, *32*, 5313─5320.

(29) Sweetnam, S.; Prasanna, R.; Burke, T. M.; Bartelt, J. A.; McGehee, M. D. How the Energetic Landscape in the Mixed Phase of Organic Bulk Heterojunction Solar Cells Evolves with Fullerene Content. *J. Phys. Chem. C*, **2016**, *120*, 6427─6434.

(30) Fichou, D. Handbook of oligo- and polythiopene, Ed., Wiley-VCH, **2008**.

(31) Liscio, A.; De Luca, G.; Nolde, F.; Palermo, V.; Mullen, K.; Samorì, P. Photovoltaic Charge Generation Visualized at the Nanoscale: A Proof of Principle. *J. Am. Chem. Soc.*, **2008**, *130*, 780─781.

(32) Nam, C. Y.; Su, D.; Black, C. T. High-Performance Air-Processed Polymer–Fullerene Bulk Heterojunction Solar Cells. *Adv. Funct. Mater*., **2009**, *19*, 3552─3559.

(33) Agostinelli, T.; Lilliu, S.; Labram, J. G.; Campoy-Quiles, M.; Hampton, M.; Pires, E.; Rawle, J.; Bikondoa, O.; Bradley, D. D. C.; Anthopoulos, T. D.; Nelson, J.; Macdonald, J. E. Real-Time Investigation of Crystallization and Phase-Segregation Dynamics in P3HT:PCBM Solar Cells During Thermal Annealing. *Adv. Funct. Mater.*, **2011**, *21*, 1701─1708.

(34) Zhong, C.; Bartelt, J. A.; McGehee, M. D.; Cao, D.; Huang, F.; Cao, Y.; Heeger, A. J. Influence of Intermixed Donor and Acceptor Domains on the Ultrafast Charge Generation in Bulk Heterojunction Materials. *J. Phys. Chem. C*, **2015**, *119*, 26889─26894.

(35) Yang, L.; Zhou, H.; You, W. Quantitatively Analyzing the Influence of Side Chains on Photovoltaic Properties of Polymer−Fullerene Solar Cells. *J. Phys. Chem. C*, **2010**, *114*, 16793─16800.

(36) Li, Y.; Chen, Y.; Liu, X.; Wang, Z.; Yang, X.; Tu, Y.; Zhu, X. Controlling Blend Film Morphology by Varying Alkyl Side Chain in Highly Coplanar Donor–Acceptor Copolymers for Photovoltaic Application. *Macromolecules*, **2011**, *44*, 6370─6381.